ARMY RESEARCH LABORATORY

Trajectory Prediction of Spin-Stabilized Projectiles With a Steady Liquid Payload

by Gene R. Cooper

ARL-TR-5810 **November 2011**

NOTICES

Disclaimers

The findings in this report are not to be construed as an official Department of the Army position unless so designated by other authorized documents.

Citation of manufacturer's or trade names does not constitute an official endorsement or approval of the use thereof.

Destroy this report when it is no longer needed. Do not return it to the originator.

Army Research Laboratory
Aberdeen Proving Ground, MD 21005-5066

ARL-TR-5810 **November 2011**

Trajectory Prediction of Spin-Stabilized Projectiles With a Steady Liquid Payload

Gene R. Cooper
Weapons and Materials Research Directorate, ARL

REPORT DOCUMENTATION PAGE	Form Approved OMB No. 0704-0188

1. REPORT DATE *(DD-MM-YYYY)*	2. REPORT TYPE	3. DATES COVERED (From - To)
November 2011	Final	October 2009–April 2011

4. TITLE AND SUBTITLE
Trajectory Prediction of Spin-Stabilized Projectiles With a Steady Liquid Payload

5a. CONTRACT NUMBER

5b. GRANT NUMBER

5c. PROGRAM ELEMENT NUMBER

6. AUTHOR(S)
Gene R. Cooper

5d. PROJECT NUMBER
AH43

5e. TASK NUMBER

5f. WORK UNIT NUMBER

7. PERFORMING ORGANIZATION NAME(S) AND ADDRESS(ES)
U.S. Army Research Laboratory
ATTN: RDRL-WML-E
Aberdeen Proving Ground, MD 21005-5066

8. PERFORMING ORGANIZATION REPORT NUMBER
ARL-TR-5810

9. SPONSORING/MONITORING AGENCY NAME(S) AND ADDRESS(ES)

10. SPONSOR/MONITOR'S ACRONYM(S)

11. SPONSOR/MONITOR'S REPORT NUMBER(S)

12. DISTRIBUTION/AVAILABILITY STATEMENT
Approved for public release; distribution is unlimited.

13. SUPPLEMENTARY NOTES

14. ABSTRACT
Payloads that behave like a liquid are carried on board some projectile configurations, and it is well established that the internal motion of a liquid payload can induce destabilizing moments on the projectile. This report creates a method to include the effect of a liquid payload in the flight dynamic equations of motion, enabling trajectory simulations of projectiles with liquid payloads. To include this effect, liquid payload moments are added to the applied loads on the projectile. These loads are computed by solving the linearized Navier-Stokes equations for a projectile undergoing coning motion. To highlight the methodology, trajectory simulation results are provided for an example projectile with different liquid payload configurations possessing stable behavior while one exhibits catastrophic flight instability.

15. SUBJECT TERMS
liquid, payload, 6-DOF, trajectory, moments

16. SECURITY CLASSIFICATION OF:			17. LIMITATION OF ABSTRACT	18. NUMBER OF PAGES	19a. NAME OF RESPONSIBLE PERSON
a. REPORT	b. ABSTRACT	c. THIS PAGE			Gene R. Cooper
Unclassified	Unclassified	Unclassified	UU	30	19b. TELEPHONE NUMBER (*Include area code*) 410-306-0787

Standard Form 298 (Rev. 8/98)
Prescribed by ANSI Std. Z39.18

Contents

List of Figures

List of Tables

INTENTIONALLY LEFT BLANK.

1. Introduction

While most projectiles in use today behave as rigid bodies while in flight, a notable number of projectiles are purposefully designed to carry a liquid payload. For example, smoke screens delivered by artillery rounds consist of a typical spin-stabilized shell containing a canister filled with white phosphorous (*1–4*). Another example is new less-than-lethal projectiles having a concentric cylindrical cavity filled with liquid that delivers this payload to a target upon impact (*5*). Finally, some projectiles are designed to be general payload delivery shells, including delivery of medical supplies, such as intravenous fluid bags (*6*).

There can be a significant difference in flight behavior between liquid- and solid-filled projectiles. The difference is caused by motion of the liquid inside the spinning projectile. This motion causes forces to act on the projectile body, which can prematurely terminate the flight by instability. Characteristics of this instability are sharp increases in angle of attack accompanied by large changes in spin rate (*7–10*). At gun launch, the motion of the projectile causes the fluid to spin up in a time-dependent manner, but it subsequently achieves steady flow.

Prediction of instability induced by a liquid payload installed in a coning projectile has been analyzed by computational fluid dynamic (CFD) simulations and with analytic linear fluid theories based on spatial-eigenvalue methods. The CFD solutions are generally best suited to liquids with a low Reynolds number (Re), while spatial-eigenvalue methods can encompass a much broader range of Re. A good survey of liquid-filled projectiles with a focus on flight instabilities is given in Sedney (*11*). Generally, analytic theories are a composition of inviscid flow and viscous boundary-layer corrections (*12–14*). The prediction of flight stability of a liquid-filled projectile has also been studied using tricyclic linear-projectile theory (*15*). This analysis assumes the effect of a liquid payload is similar to the Magnus effect. Spectral analysis used to numerically compute liquid-fill induced moments has been incorporated into six-degree-of-freedom (6-DOF) simulations (*16*). The angular motion of a low-Re liquid-filled projectile has also been simulated using a precomputed table of liquid moments, obtained from CFD, in 6-DOF calculations (*17*).

The present report meshes a well-developed spatial-eigenvalue theory directly into a standard 6-DOF projectile flight dynamic model. Hence, a well-established rotating liquid model calculates liquid moments at each time step of the 6-DOF trajectory numerical simulation without the need of interpolation to gain the effects of liquid payloads. This report further bridges the gap between the body of literature on effects of viscous liquid payloads on projectiles and 6-DOF projectile flight dynamic modeling. The report begins with a review of rigid projectile flight dynamic modeling along with a description of modeling a rotating liquid in a cylindrical cavity. The two models are subsequently integrated such that a projectile flight dynamic model with a liquid payload results. To highlight the utility of the methodology, the

flight dynamic model is exercised on an example shell. Comparisons are made between a liquid-filled projectile and a similar solid-filled projectile highlighting the predictive capability of the new model.

2. Projectile Flight Dynamic Model With a Liquid Payload

A typical 6-DOF rigid projectile model is employed to predict the dynamics of a projectile in flight. These equations assume a flat Earth. The well-known 6-DOF states comprise the three translational components describing the position of the projectile's center of mass and the three Euler angles describing the orientation of the projectile with respect to the Earth. Figures 1 and 2 provide a visualization of the degrees of freedom.

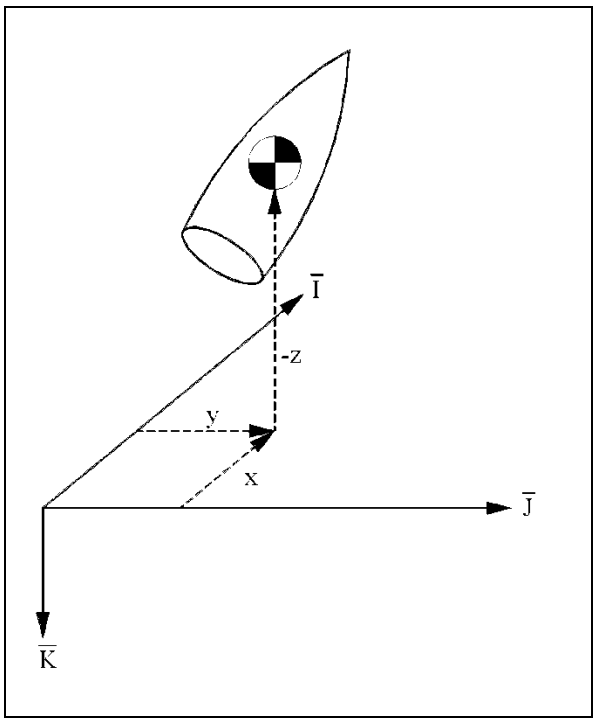

Figure 1. Projectile position coordinate definitions.

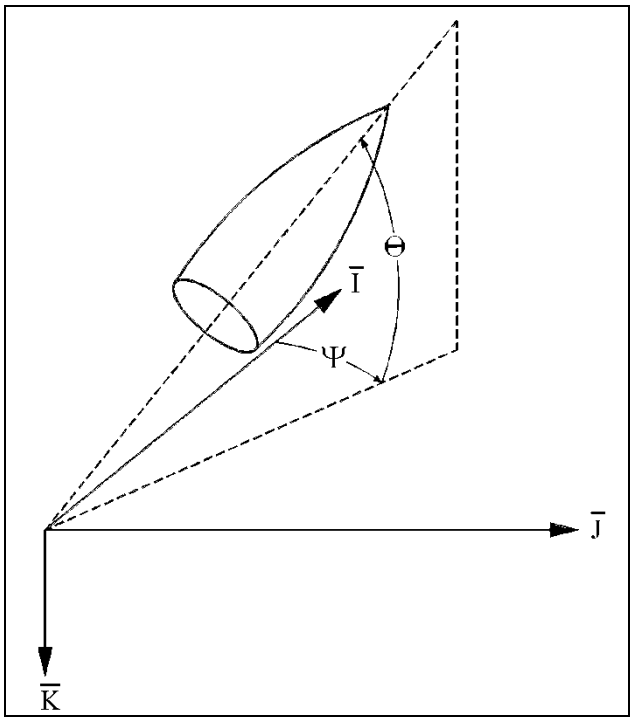

Figure 2. Projectile orientation definitions.

The equations of motion (*18*) derived in the no-roll frame are shown in equations 1–4.

$$\begin{Bmatrix} \dot{x} \\ \dot{y} \\ \dot{z} \end{Bmatrix} = \begin{bmatrix} c_\theta c_\psi & -s_\psi & s_\theta c_\psi \\ c_\theta s_\psi & c_\psi & s_\theta s_\psi \\ -s_\theta & 0 & c_\theta \end{bmatrix} \begin{Bmatrix} \tilde{u} \\ \tilde{v} \\ \tilde{w} \end{Bmatrix}. \tag{1}$$

$$\begin{Bmatrix} \dot{\phi} \\ \dot{\theta} \\ \dot{\psi} \end{Bmatrix} = \begin{bmatrix} 1 & 0 & t_\theta \\ 0 & 1 & 0 \\ 0 & 0 & 1/c_\theta \end{bmatrix} \begin{Bmatrix} \tilde{p} \\ \tilde{q} \\ \tilde{r} \end{Bmatrix}. \tag{2}$$

$$\begin{Bmatrix} \dot{\tilde{u}} \\ \dot{\tilde{v}} \\ \dot{\tilde{w}} \end{Bmatrix} = \begin{Bmatrix} \tilde{X}/m \\ \tilde{Y}/m \\ \tilde{Z}/m \end{Bmatrix} - \begin{bmatrix} 0 & -\tilde{r} & \tilde{q} \\ \tilde{r} & 0 & \tilde{r}t_\theta \\ -\tilde{q} & -\tilde{r}t_\theta & 0 \end{bmatrix} \begin{Bmatrix} \tilde{u} \\ \tilde{v} \\ \tilde{w} \end{Bmatrix}. \tag{3}$$

$$\begin{Bmatrix} \dot{\tilde{p}} \\ \dot{\tilde{q}} \\ \dot{\tilde{r}} \end{Bmatrix} = [I]^{-1} \left(\begin{Bmatrix} \tilde{L} \\ \tilde{M} \\ \tilde{N} \end{Bmatrix} - \begin{bmatrix} 0 & -\tilde{r} & \tilde{q} \\ \tilde{r} & 0 & \tilde{r}t_\theta \\ -\tilde{q} & -\tilde{r}t_\theta & 0 \end{bmatrix} [I] \begin{Bmatrix} \tilde{p} \\ \tilde{q} \\ \tilde{r} \end{Bmatrix} \right). \tag{4}$$

Note that the following shorthand notation for trigonometric functions is used in equations 1–4: $s_\alpha = \sin(\alpha)$, $c_\alpha = \cos(\alpha)$, and $t_\alpha = \tan(\alpha)$.

The force acting on the projectile in equation 3 comprises the weight force (W) and the aerodynamic force. The aerodynamic force is split into a standard force (A) and a Magnus force (M). The combination of forces is expressed in equation 5.

$$\begin{Bmatrix} \tilde{X} \\ \tilde{Y} \\ \tilde{Z} \end{Bmatrix} = \begin{Bmatrix} \tilde{X}_W \\ \tilde{Y}_W \\ \tilde{Z}_W \end{Bmatrix} + \begin{Bmatrix} \tilde{X}_A \\ \tilde{Y}_A \\ \tilde{Z}_A \end{Bmatrix} + \begin{Bmatrix} \tilde{X}_M \\ \tilde{Y}_M \\ \tilde{Z}_M \end{Bmatrix}. \tag{5}$$

Equation 6 provides the expression for the weight force in the no-roll coordinate system.

$$\begin{Bmatrix} \tilde{X}_W \\ \tilde{Y}_W \\ \tilde{Z}_W \end{Bmatrix} = mg \begin{Bmatrix} -s_\theta \\ 0 \\ c_\theta \end{Bmatrix}. \tag{6}$$

Equation 7 provides the expression for the aerodynamic force in the no-roll coordinate system. This force acts upon the projectile at the aerodynamic center of pressure.

$$\begin{Bmatrix} \tilde{X}_A \\ \tilde{Y}_A \\ \tilde{Z}_A \end{Bmatrix} = -\frac{\pi}{8}\rho V^2 D^2 \begin{Bmatrix} C_{X0} + C_{X2}\left(\tilde{v}^2 + \tilde{w}^2\right)/V^2 \\ C_{Y0} + C_{n\alpha}\tilde{v}/V \\ C_{Z0} + C_{n\alpha}\tilde{w}/V \end{Bmatrix}. \tag{7}$$

Equation 8 provides the expression for the Magnus force in the no-roll coordinate system. The Magnus force acts upon the projectile at the Magnus force center of pressure.

$$\begin{Bmatrix} \tilde{X}_M \\ \tilde{Y}_M \\ \tilde{Z}_M \end{Bmatrix} = \frac{\pi}{8}\rho V^2 D^2 \begin{Bmatrix} 0 \\ \dfrac{\tilde{p} D C_{N_{P\alpha}} \tilde{w}}{2V^2} \\ \dfrac{-\tilde{p} D C_{N_{P\alpha}} \tilde{v}}{2V^2} \end{Bmatrix}. \tag{8}$$

Equations 7 and 8 are based on Mach number–dependent coefficients and the total aerodynamic velocity given in equation 9.

$$V = \sqrt{\tilde{u}^2 + \tilde{v}^2 + \tilde{w}^2}\,. \tag{9}$$

The moment acting on the projectile in equation 4 comprises the moment due to the standard aerodynamic force (A), the moment due to the Magnus aerodynamic force (M), the unsteady aerodynamic moment (UA), and the liquid payload moment (L) as shown in equation 10.

$$\begin{Bmatrix} \tilde{L} \\ \tilde{M} \\ \tilde{N} \end{Bmatrix} = \begin{Bmatrix} \tilde{L}_A \\ \tilde{M}_A \\ \tilde{N}_A \end{Bmatrix} + \begin{Bmatrix} \tilde{L}_M \\ \tilde{M}_M \\ \tilde{N}_M \end{Bmatrix} + \begin{Bmatrix} \tilde{L}_{UA} \\ \tilde{M}_{UA} \\ \tilde{N}_{UA} \end{Bmatrix} + \begin{Bmatrix} \tilde{L}_L \\ \tilde{M}_L \\ \tilde{N}_L \end{Bmatrix}. \tag{10}$$

The moment due to the aerodynamic force is expressed in equation 11.

$$\begin{Bmatrix} \tilde{L}_A \\ \tilde{M}_A \\ \tilde{N}_A \end{Bmatrix} = \begin{bmatrix} 0 & -R_{CZ} & R_{CY} \\ R_{CZ} & 0 & -R_{CX} \\ -R_{CY} & R_{CX} & 0 \end{bmatrix} \begin{Bmatrix} \tilde{X}_A \\ \tilde{Y}_A \\ \tilde{Z}_A \end{Bmatrix}. \tag{11}$$

The moment due to the Magnus force is expressed in equation 12.

$$\begin{Bmatrix} \tilde{L}_M \\ \tilde{M}_M \\ \tilde{N}_M \end{Bmatrix} = \begin{bmatrix} 0 & -R_{MZ} & R_{MY} \\ R_{MZ} & 0 & -R_{MX} \\ -R_{MY} & R_{MX} & 0 \end{bmatrix} \begin{Bmatrix} \tilde{X}_M \\ \tilde{Y}_M \\ \tilde{Z}_M \end{Bmatrix}. \tag{12}$$

The unsteady aerodynamic moments acting on the projectile are expressed in equation 13.

$$\begin{Bmatrix} \tilde{L}_{UA} \\ \tilde{M}_{UA} \\ \tilde{N}_{UA} \end{Bmatrix} = \frac{\pi}{8} \rho V^2 D^3 \begin{Bmatrix} C_{DD} + \frac{\tilde{p} D C_{LP}}{2V} \\ \frac{\tilde{q} D C_{MQ}}{2V} \\ \frac{\tilde{r} D C_{MQ}}{2V} \end{Bmatrix}. \tag{13}$$

The coefficients used in this model are specific functions of the Mach number of the projectile. For fin-stabilized projectiles, Magnus force and moment are typically ignored since its effect is rather small for slowly rolling projectiles.

The angular motion of a projectile is altered by the inertial waves propagating through the liquid payload. In turn, these waves act on the walls of the liquid cavity and generate a liquid moment. The impact of this moment can have a devastating impact on the projectile's angular motion (*19–21*). For this report, the liquid moment is calculated from steady linear-projectile theory, which incorporates solutions of the linearized Navier-Stokes equations (*18*). In general, this liquid moment model is a linear combination of fast and slow mode liquid moment contributions. In section 2 of his report, Murphy (*19*) states that for a steady-state coning projectile with a liquid payload, ". . . only the fast mode motion is adversely affected by the liquid side moment." For this reason, only the fast coning mode is used to calculate the liquid moment in this paper.

Figure 3 shows the orientation of body unit vectors (I_B , J_B , K_B) to velocity unit vectors (I_V , J_V , K_V). Appling the liquid theory (*18*) to figure 3 allows the liquid transverse and roll liquid moments to be written as shown in equation 14.

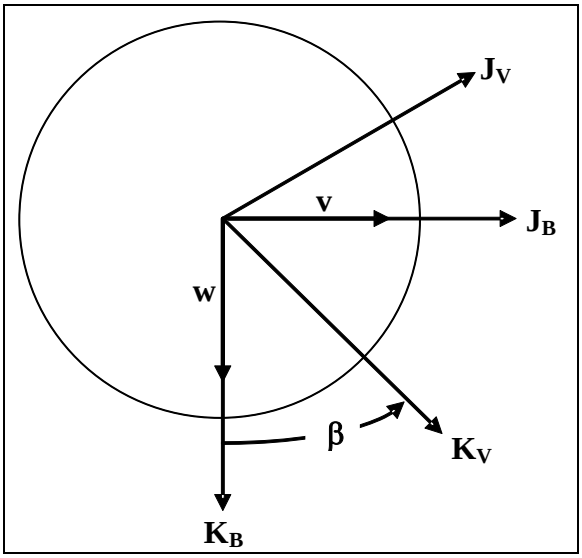

Figure 3. Liquid transverse velocity orientation definitions.

$$\begin{bmatrix} \tilde{L}_L \\ \tilde{M}_L \\ \tilde{N}_L \end{bmatrix} = m_L a^2 \tilde{p}^2 T \begin{bmatrix} 1 & 0 & 0 \\ 0 & c_{\beta-\phi} & s_{\beta-\phi} \\ 0 & -s_{\beta-\phi} & c_{\beta-\phi} \end{bmatrix} \begin{bmatrix} K^2 C_{LRM} \\ K C_{LSM} \\ K C_{LIM} \end{bmatrix}$$

$$C_{LRM} = -C_{LSM} + \frac{T\varepsilon}{2}\left(1 - \frac{4}{3}\left(\frac{c}{a}\right)^2\right) \quad . \tag{14}$$

$$K = \frac{\sqrt{\tilde{v}^2 + \tilde{w}^2}}{V}, \ \beta = \frac{\tilde{v}}{\tilde{w}}$$

The moment coefficients C_{LSM} and C_{LIM} depend on the fast mode coning frequency T, fast mode undamping ε, the cavity aspect ratio c/a, liquid Re, and the magnitude of axial spin (*19*). Values of the fast mode pair (T, ε) are obtained from equation 15.

$$T = \frac{\sqrt{2\tilde{p}^2\left(I_X + a^2 m_L C_{LIM}\right)^2 - \pi\rho C_{NA} D^2 I_Y R_{CX} V^2}}{2\sqrt{2}\tilde{p} I_Y} + \frac{I_X + a^2 m_L C_{LIM}}{2I_Y}$$

$$\varepsilon = \frac{\pi\rho D^2\left(\frac{D\left(C_{MQ}T + C_{YPA}R_{MX}\right)}{2} - \frac{C_{NA}\left(I_Y T - I_X\right)}{M}\right)V}{8\tilde{p}T\left(2I_Y T - I_X\right)} + \frac{a^2 m_L C_{LSM}}{\left(2I_Y T - I_X\right)} \quad . \tag{15}$$

The liquid moment coefficients C_{LSM} and C_{LIM} are calculated using the techniques given by Murphy (*19*).

3. Results

The example simulations given here consider liquid payloads in a typical projectile with launch properties given in table 1.

Table 1. Launch properties of projectile.

Physical Parameters	Magnitude
Ix	0.1157 slug ft^2
Iy, Iz	1.1972 slug ft^2
m	103.0 lb/ft
D	0.510 ft
Launch velocity, V	2460.0 ft s^{-1}
Launch axial spin rate, p	1500.0 s^{-1}

The liquid density ρ_L is taken to be 3.5 times the density of liquid water, and the viscosity υ is selected such that launch Re $\geq 8 \times 10^6$. This is sufficient to ensure that the Re remains large so boundary layer analysis (*18*) adequately governs the liquid physics for the entire trajectory. The liquid cavity is a cylinder with aspect ratio c/a = 3.75 completely filled with this low-viscosity liquid. Figure 4 shows the range of nondimensional coning frequencies, T, for a typical trajectory of this projectile housing a frozen (solid) liquid payload.

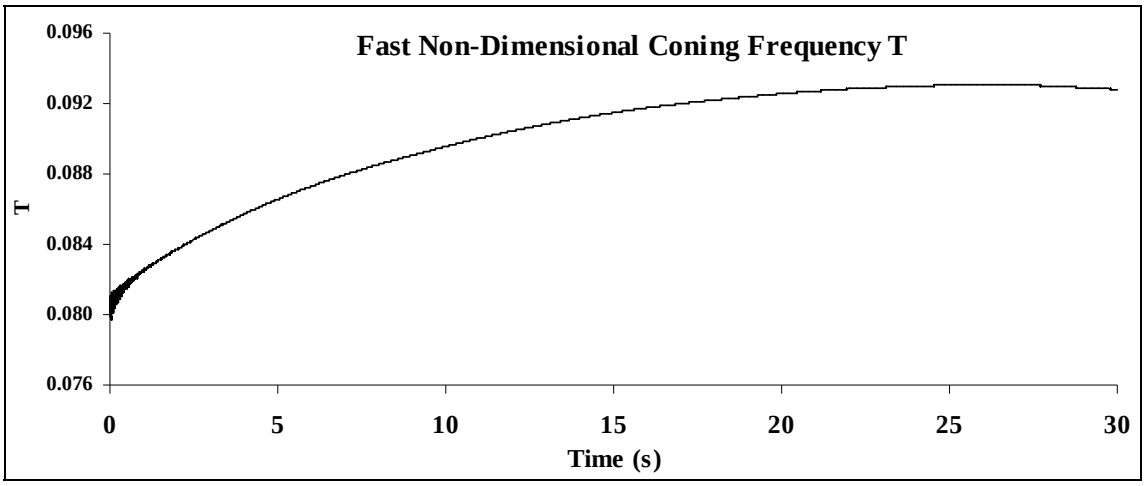

Figure 4. Nondimensional fast mode coning frequencies.

The Re for a given aspect ratio can cause large variations in the liquid moment when subjected to a range of nondimensional coning frequencies. Applying steady-state linear liquid theory to a payload configuration undergoing coning motion reveals in figure 5 the side moment coefficient C_{LSM} with c/a = 3.75 for two numbers $Re = 8 \times 10^6$ and 8×10^8. These results depict important C_{LSM} behavior, where the peaks indicate a potential problem due to large liquid moments when the nondimensional coning rate $T \approx 0.088$. Note the amplitude of the peak has a strong dependence on Re. Peak values of C_{LSM} are nearly 2 orders of magnitude larger than the nonpeak values of C_{LSM}.

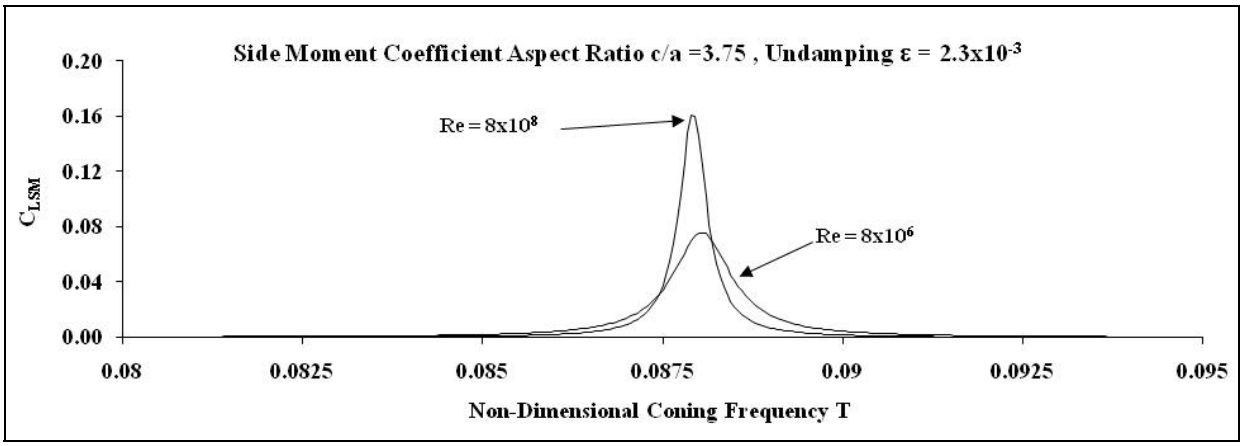

Figure 5. C_{LSM} vs. coning frequency and Re, resonance $T \approx 0.088$.

Figure 5 suggests that for a sufficiently large Re, a free-flight missile having nondimensional coning frequencies in the neighborhood of T = 0.088 will experience a significantly larger liquid moment than it does for frequencies outside this neighborhood. Such results are characteristic of the root cause of projectile instabilities due to liquid payloads. The aspect ratio, coupled with a large enough Re, forces inertial waves in the coning fluid to generate large C_{LSM} coefficients (*19*). In general, increasing Re causes the liquid side moment to increase near T = 0.088, and this pronounced peak signifies a possible resonant frequency. This is one indicator of a liquid payload possibly causing the fast coning frequencies to change such that an instability occurs near T = 0.088. Note the range of frequencies given in figure 5 is close to the fast mode T frequencies for the frozen liquid found in figure 4.

Next a series of results showing the effect a liquid payload has on projectile angular motion during flight is shown. Results presented here are for a launch $Re = 8 \times 10^6$, which is large enough so linear liquid theory with boundary layer corrections is valid throughout the entire trajectory. Figures 6 and 7 compare roll moment and spin rate results for a frozen liquid and a flowing liquid. These variables are selected because the rotational physics of a projectile causing a rapid decrease in spin rate is a strong indicator of flight instability caused by liquid payloads (*18*).

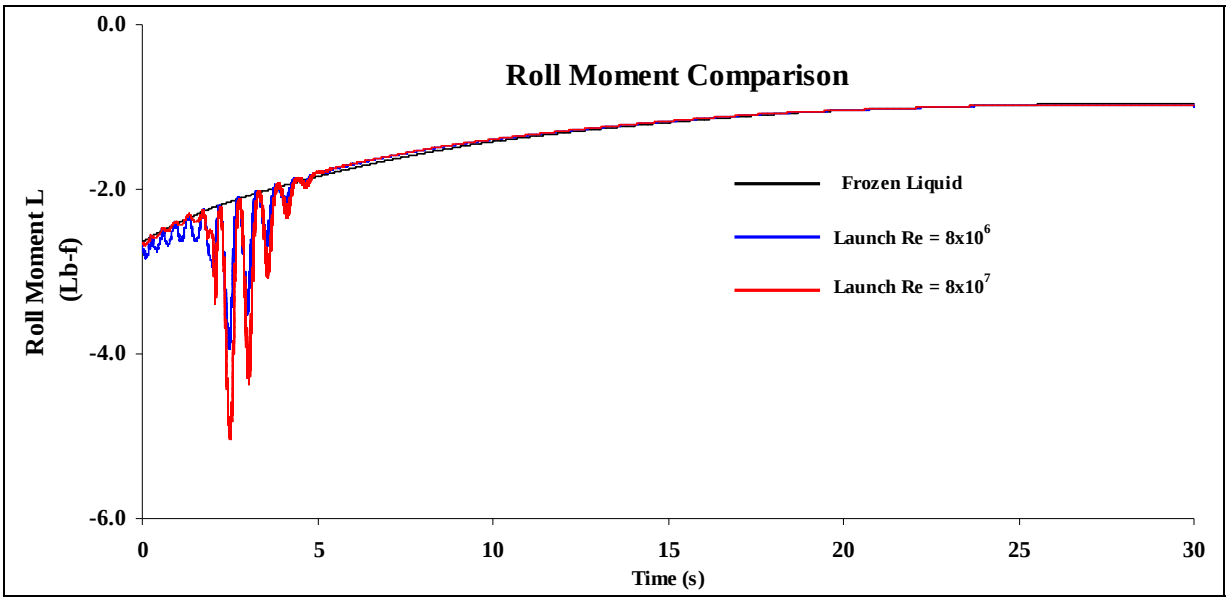

Figure 6. Projectile roll moment for frozen and flowing liquid payloads.

The liquid payloads for the launch Re chosen in these examples has small effects on liquid roll moment, as shown in figure 6. As expected, figure 7 shows the projectile roll rates also change slightly compared to the frozen liquid payload.

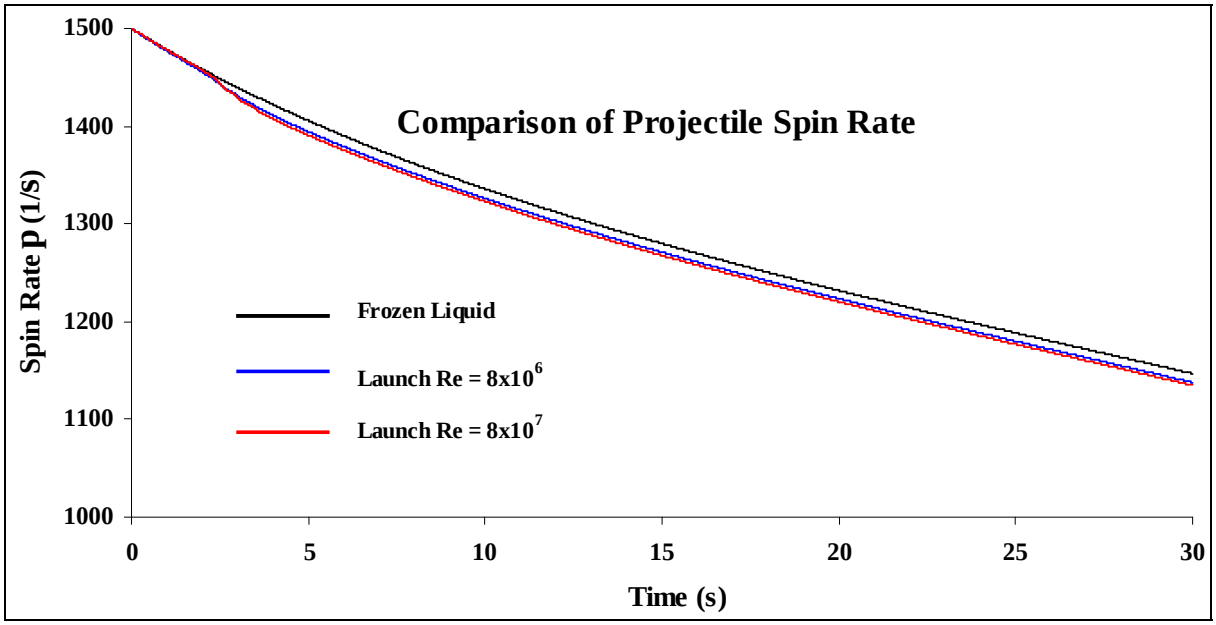

Figure 7. Projectile spin rate for frozen and flowing liquid payloads.

Evidently the increased magnitude of the projectile roll moment due to the flowing liquid is not sufficient to cause flight instability since the roll performance of the projectile changes very little.

The liquid side moment coefficient, C_{LSM}, is an important parameter when evaluating the impact a liquid payload has on projectile angular motion. Figure 8 shows the fast mode liquid moment coefficient as a function of T. This chart shows that C_{LSM} changes rapidly for the region $0.086 \le T \le 0.090$, and the magnitudes of C_{LSM} exhibits the approximation $C_{LSM} \sim \sqrt{Re}$ (*18*) when the coning rate is in the neighborhood of T = 0.088.

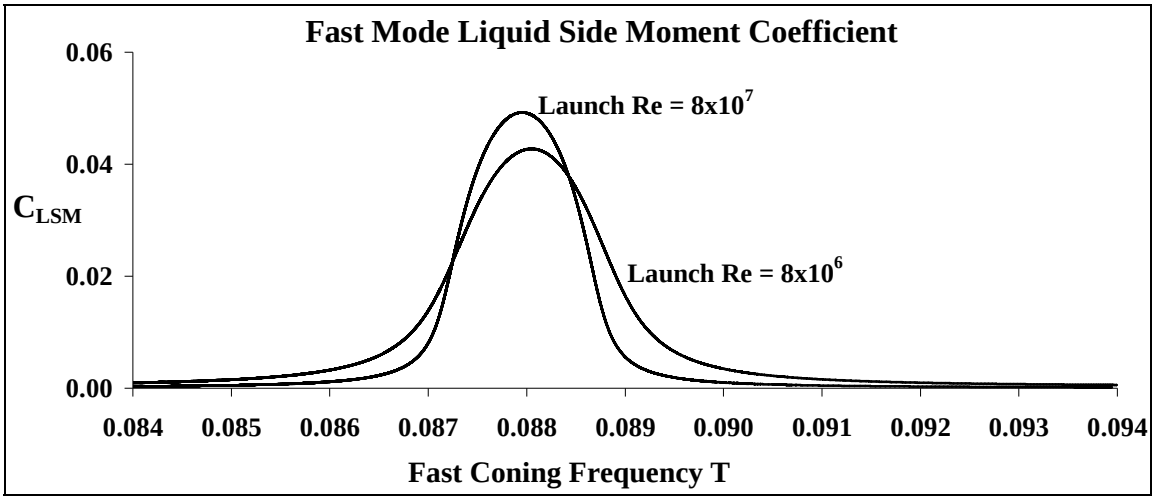

Figure 8. Liquid moment coefficients vs. nondimensional fast mode frequency.

Figure 9 compares the angle of attack (AOA) for identical projectiles with payloads supporting inertial waves and frozen liquid payloads.

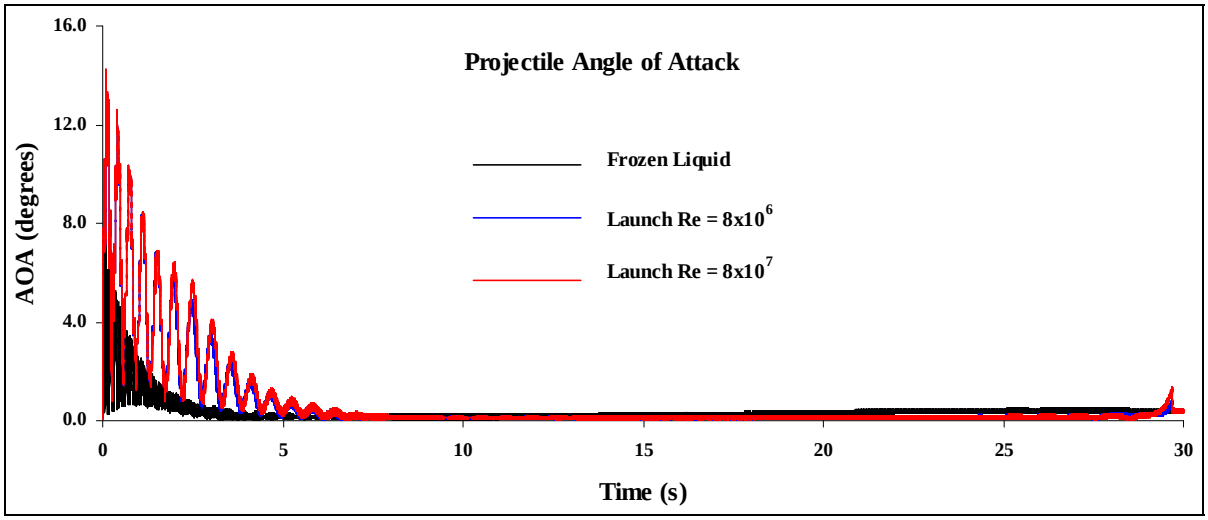

Figure 9. Comparison of AOA of frozen and liquid payloads.

Apparently the inertial wave motion slightly increases the AOA for a liquid with launch Re of 8.0×10^6 or 8.0×10^7 compared to the frozen liquid, but this increase is not enough to cause concern of flight instability. In fact, the results presented so far show no indication of flight instability even when the projectile has a coning rate near T = 0.088 for the potential problem in C_{LSM} found in figures 5 and 8.

In order to understand the dynamics of a liquid-filled projectile exhibiting angular instability, we consider figure 4 and exploit the peak value of C_{LSM} near T = 0.088. Thus, to substantially increase the size of the liquid moment, we assume the payload comprises a hypothetical liquid with a decreased viscosity so that the launch Re is large enough to cause substantial increases in liquid side moment during flight. In particular, we want this liquid to generate large enough values of C_{LSM} for $T \approx 0.088$ to alter the angular motion of the projectile. A sufficiently large decrease in projectile spin rate along with a large increase in AOA suggests the hypothetical liquid may cause premature termination of flight. Figure 10 shows the fast nondimensional T dependence of the side moment coefficient, C_{LSM}, rapidly increasing near T = 0.088 for launch $Re = 4 \times 10^8$. This indicates a possible increase in the magnitude of projectile angular motion, which is consistent with the resonance configuration presented in figure 5.

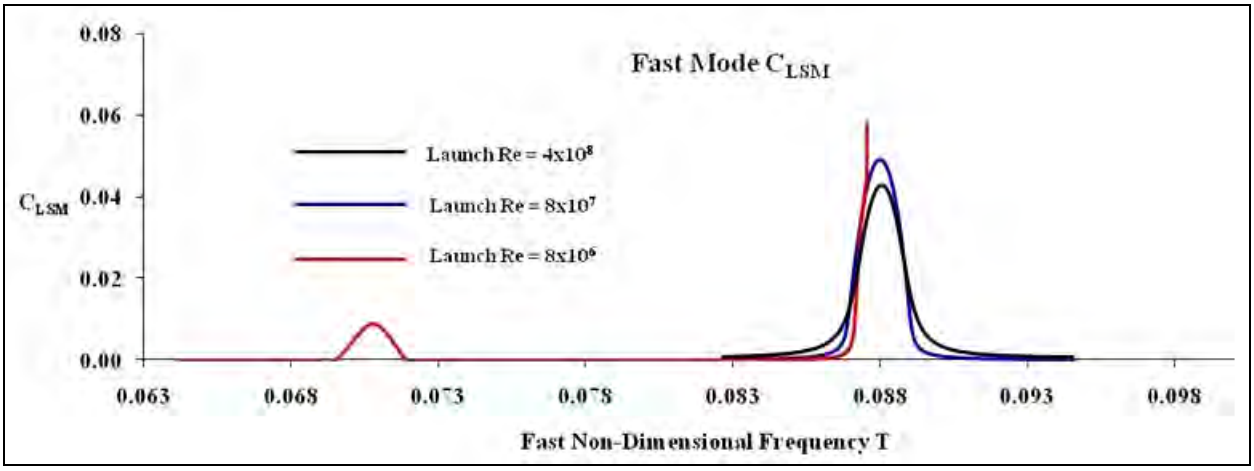

Figure 10. Comparison of projectile roll moment vs. payload launch Re.

Figure 11 compares the AOA of the projectile with liquid payloads having three different launch Re's.

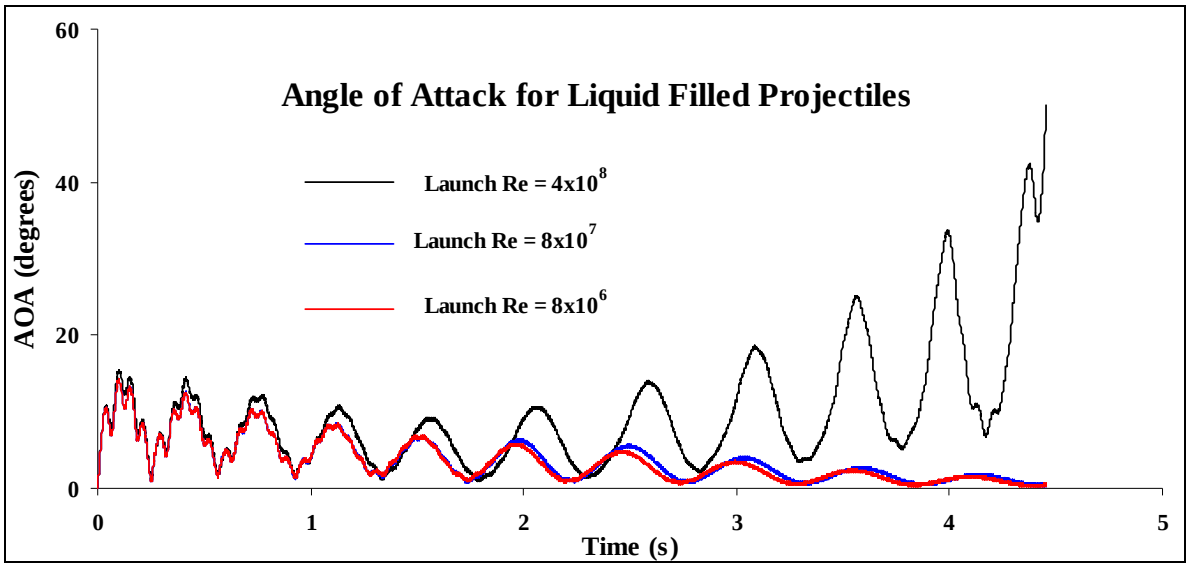

Figure 11. Projectile AOA vs. launch Re of liquid payload.

The projectile with launch Re = 4×10^8 causes the fast frequency at $t \approx 4.5$ s, $T \approx 0.088$, to generate an AOA >50° for which the judgment was made to terminate the numerical integration. Figure 12 shows the corresponding projectile roll moment L rapidly increasing in magnitude due to the larger Re. Note that in the neighborhood of T = 0.088, the fast mode liquid motion is responsible for increasing the magnitude of L.

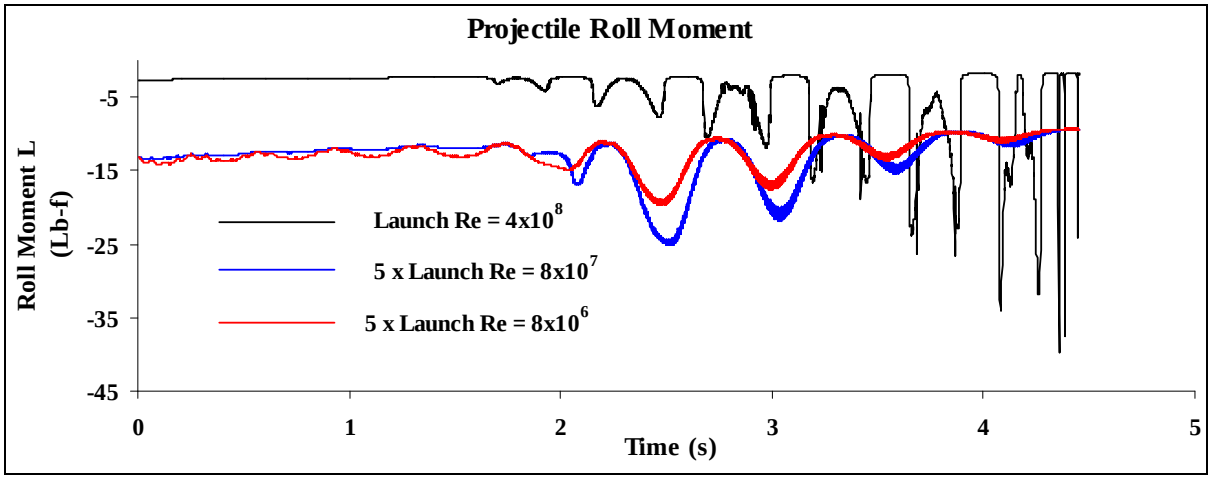

Figure 12. Comparison of projectile roll moment vs. launch Re.

Figure 13 shows the corresponding projectile roll rates for the launch Re = 8×10^6 and 4×10^8, which correlates with the size of liquid moment coefficient C_{LRM} as shown in equation 15. The increase in $|L|$ for Re = 4×10^8 causes the rapid decrease in roll rate.

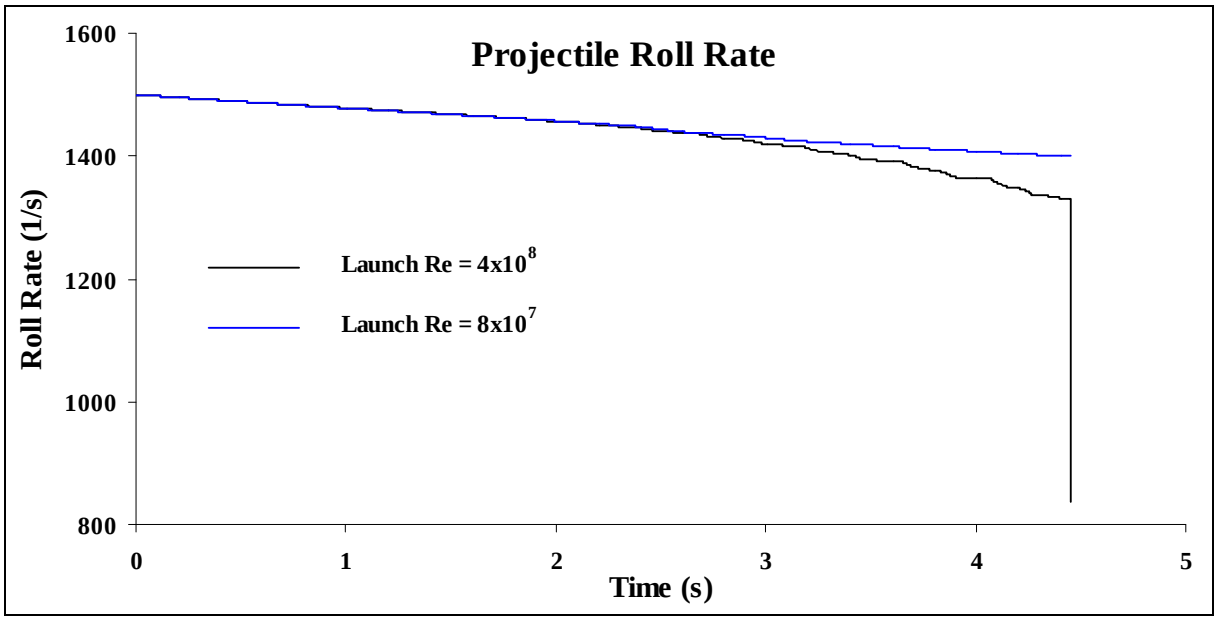

Figure 13. Comparison of roll rate due to payload launch Re.

Figure 14 compares corresponding pitch rates of the frozen liquid and launch Re = 4×10^8 configurations. The rapid increase in q values near $t \approx 4.5$ s is caused by the fast mode liquid side moment.

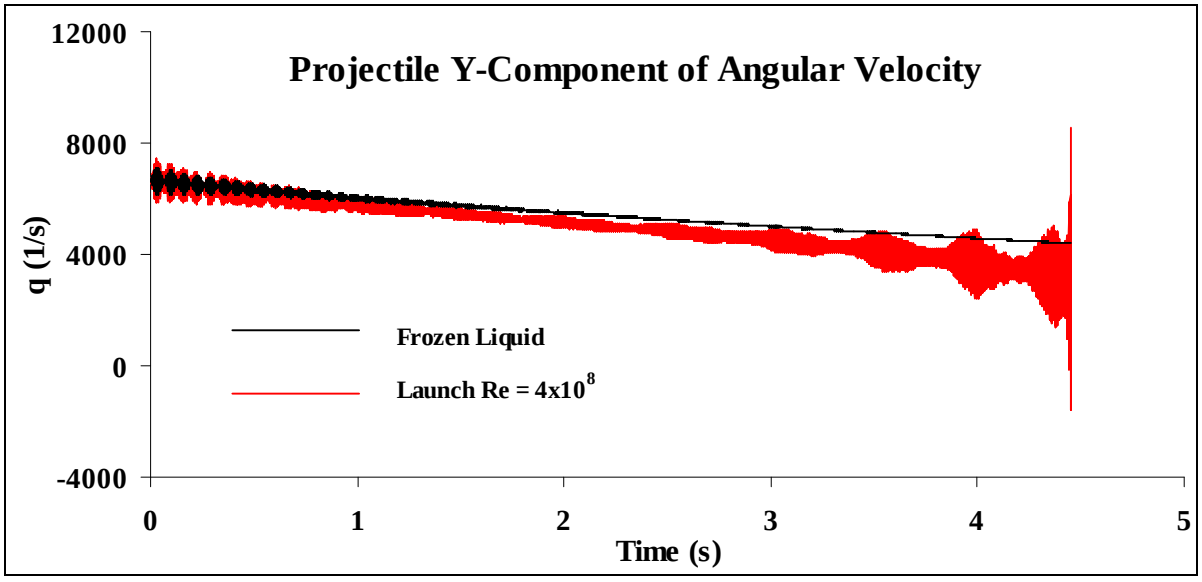

Figure 14. Comparison of pitch rates due to frozen and liquid payload.

A contrast in projectile yaw rates for frozen and liquid payload is given in figure 15. Again the rapid increase in yaw rate takes place near t ≈ 4.5 s in the neighborhood of the fast mode resonance.

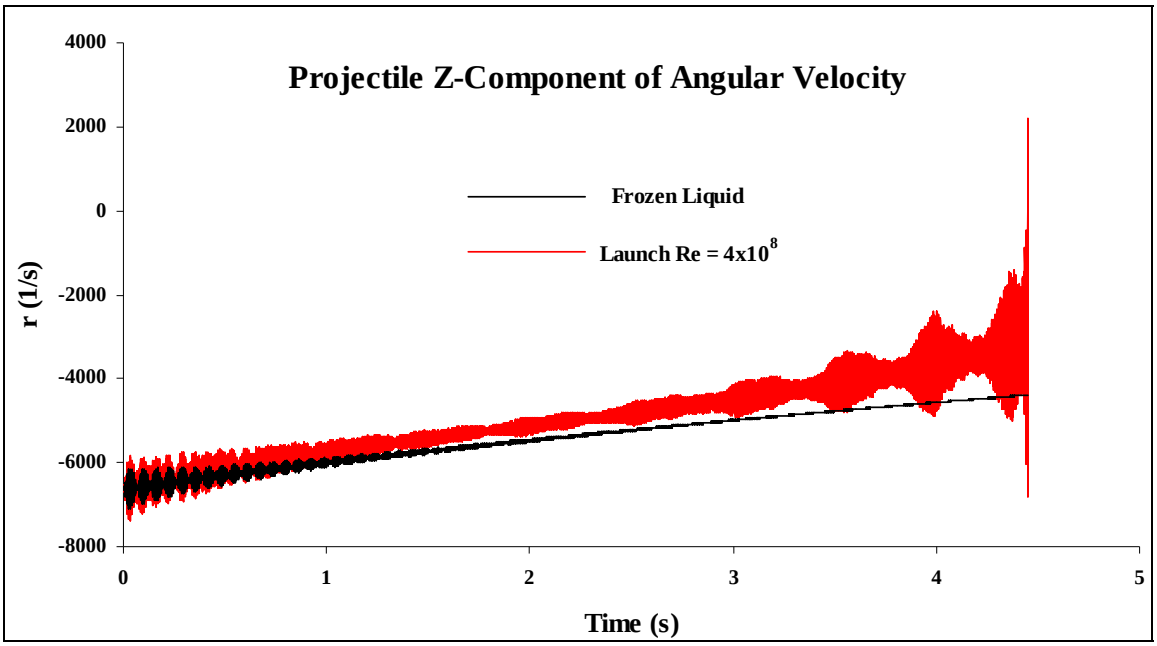

Figure 15. Comparison of yaw rates due to frozen and liquid payloads.

These calculations show a significant difference in projectile angular motion when the liquid payload has a launch Re = 4×10^8 compared to the same projectile with a frozen liquid.

4. Conclusion

An integrated trajectory simulation for a projectile with an internal liquid payload has been created and exercised. The liquid moments are calculated using linear liquid theory applied to a low-viscosity liquid undergoing two-mode steady state coning motion. High Re boundary layers approximate the liquid shear moment, yielding an average quasi-static liquid moment that is applied to a nonlinear 6-DOF time-dependent trajectory model. These quasi-static averages yield approximate predictions describing the motion of projectiles with low-viscosity liquid payloads filling a cylindrical cavity. The nonlinear 6-DOF motion of a projectile is often well approximated as the sum of fast and slow coning motions. Thus, under these conditions the linear liquid analysis can predict when a projectile exhibits flight instability due to a liquid payload by tracking the coning frequencies during the 6-DOF numerical integration process.

Calculations presented in this report show how both stable and unstable liquid payload configurations influence trajectory flight parameters. Unstable liquid payload configurations result from an improper combination of liquid Re's, payload geometry, and quasi-static projectile coning mode rates. In such cases, projectile roll rate and axial moment decrease rapidly due to the quasi-static liquid moment.

5. References

1. D'Amico, W. P.; Mark, A. *The Application of a Highly Permeable Medium to Reduce Spin-Up Time and to Stabilize a Liquid-Filled Shell*; BRL-MR-02851; U.S. Army Ballistic Research Laboratory: Aberdeen Proving Ground, MD, July 1978.

2. D'Amico, W. P.; Clay, W. H. *Flight Tests for Prototype Felt Wedge/White Phosphorous Improved Smoke Concept*; BRL-MR-02824; U.S. Army Ballistic Research Laboratory: Aberdeen Proving Ground, MD, April 1978.

3. Cooper, G. R. *Moment Exerted on a Coning Projectile by a Spinning Liquid in a Cylindrical Cavity Containing a Porous Medium*; BRL-MR-3677; U.S. Army Ballistic Research Laboratory: Aberdeen Proving Ground, MD, June, 1988.

4. Cooper, G. R. Spinning Projectile With an Inviscid Liquid Payload Impregnating Porous Media. *American Institute of Aeronautics and Astronautics (AIAA) Journal* **March 2008**, *46* (3), 783–787.

5. Cooper, G. R. *Moments on a Coning M864 by a Liquid Payload: The Candlestick Problem and Porous Media*; ARL-TR-3837; U.S. Army Research Laboratory: Aberdeen Proving Ground, MD, July 2006.

6. Dean, C.; Weber, D.; Molnar, J.; Hollis, M.; D'Amico, W.; Brandon, F.; Davis, B. *Savage Medical Resupply Projectile*; U.S. Army Armament Munitions: Aberdeen Proving Ground, MD, October 1996.

7. Stewartson, K. On the Stability of a Spinning Top Containing Liquid. *Journal of Fluid Mechanics* **1959**, *5* (4), 577–592.

8. Karpov, B. G. *Experimental Observation of the Dynamic Behavior of Liquid Filled Shell*; BRL Report 1171; U.S. Army Ballistic Research Laboratory: Aberdeen Proving Ground, MD, August 1961.

9. Mark, A.; Mermagen, W. H. *Measurement of Spin Decay and Instability of Liquid-Filled Projectiles via Telemetry*; BRL Memorandum Report 2333; U.S. Army Ballistic Research Laboratory: Aberdeen Proving Ground, MD, October 1973.

10. Kitchens, C. W., Jr.; Gerber, N.; Sedney, R. *Spin Decay of Liquid-Filled Projectiles*; *Journal of Spacecraft and Rockets* **November–December 1978**, *15*, 348–354.

11. Sedney, R. A Survey of the Fluid Dynamic Aspects of Liquid-Filled Projectiles. *Proceedings of the AIAA 12th AFM*; AIAA Paper AIAA-85-1822-CP; Snowmass, CO, August 1985.

12. Wedemeyer, E. H. *Viscous Corrections to Stewartson's Stability Criterion*; BRL Report 1325; U.S. Army Ballistic Research Laboratory: Aberdeen Proving Ground, MD, June 1966.

13. Kitchens, C. W., Jr.; Gerber, N.; Sedney, R. *Oscillations of a Liquid in a Rotating Cylinder: Part I. Solid-Body Rotation*; BRL-TR-02081; U.S. Army Ballistic Research Laboratory: Aberdeen Proving Ground, MD, June 1978.

14. Frasier, J. T.; Scott, W. E. Stability of a Liquid-Filled Gyroscope: Inviscid Analysis, Viscous Correction, and Experiments. *Journal of Spacecraft and Rockets* **May 1971**, *8* (5), 523–526.

15. Weber, D. J. Simplified Method for Evaluating the Flight Stability of Liquid-Filled Projectiles. *Journal of Spacecraft and Rockets* **1994**, *31* (1), 130–134.

16. Thorwald, H. Flight Simulation for Liquid-Filled Projectiles. *Proceedings of the 1987 Scientific Conference on Chemical Defense Research*; CRDEC-SP-88013; June 1988; pp 378–385.

17. Vaughn, H. R.; Wolfe, W. P.; Oberkampf, W. L. Flight Trajectory Simulation of Fluid Payload Projectiles. *Journal of Guidance, Control and Dynamics* **March-April 1986**, *9* (2), 213–220.

18. Slegers, N.; Kyle, J.; Costello, M. Nonlinear Model Predictive Control Technique for Unmanned Air Vehicles. *Journal of Guidance Control and Dynamics* **2006**, *29* (5), 1179–1188.

19. Murphy, C. H. Angular Motion of a Spinning Projectile With a Viscous Liquid Payload; BRL-MR-3194; U.S. Army Ballistic Research Laboratory: Aberdeen Proving Ground, MD, August 1982. Also see *Journal of Guidance, Control and Dynamics* **July–August 1983**, *6*, (4), 280–286.

20. Murphy, C. H. A Relation Between Liquid Roll Moment and Liquid Side Moment. *Journal of Guidance, Control and Dynamics* **March–April 1985**, *8* (2), 287–288.

21. Murphy, C. H.; Bradley, J. W.; Mermagen, W. H. Side Moment Exerted by a Spinning Coning Highly Viscous Liquid Payload; BRL Technical Report 3074; U.S. Army Ballistic Research Laboratory: Aberdeen Proving Ground, MD, December 1989.

INTENTIONALLY LEFT BLANK.

List of Symbols, Abbreviations, and Acronyms

6-DOF	six degrees of freedom
a	radius of cylinder containing fluid (ft)
AOA	angle of attack
c	half length of the cylinder containing N subcylinders (ft)
C_{dd}	aero-coefficients
CFD	computational fluid dynamics
I	projectile moment of inertia $I=\begin{Bmatrix} I_X & 0 & 0 \\ 0 & I_Y & 0 \\ 0 & 0 & I_Y \end{Bmatrix}$ (slug ft^2)
m	projectile mass (slug)
m_L	liquid mass $m_L = 2\pi a^2 c\rho$ (slug)
$\begin{Bmatrix} \tilde{L} \\ \tilde{M} \\ \tilde{N} \end{Bmatrix}$	projectile moment (ft lbf)
$\begin{Bmatrix} \tilde{p} \\ \tilde{q} \\ \tilde{r} \end{Bmatrix}$	projectile angular velocity (s^{-1})
$\begin{Bmatrix} R_{dX} \\ R_{dY} \\ R_{dZ} \end{Bmatrix}$	displacement of d relative to mass center coordinates (ft)
Re	Reynolds number, $a^2\tilde{p}/\nu$
s_g	gyroscopic stability factor
t	time (s)
T	nondimensionalized coning frequency

$\begin{Bmatrix} \tilde{u} \\ \tilde{v} \\ \tilde{w} \end{Bmatrix}$ nonrolling projectile velocity $\begin{bmatrix} \tilde{u} \\ \tilde{v} \\ \tilde{w} \end{bmatrix} = \begin{bmatrix} \text{axial velocity} \\ \text{radial velocity} \\ \text{azimuthal velocity} \end{bmatrix}$ (ft s^{-1})

$\begin{Bmatrix} u \\ v \\ w \end{Bmatrix}$ projectile mass center velocity $\begin{bmatrix} u \\ v \\ w \end{bmatrix} = \begin{bmatrix} \text{axial velocity} \\ \text{radial velocity} \\ \text{azimuthal velocity} \end{bmatrix}$ (ft s^{-1})

$\begin{Bmatrix} x \\ y \\ z \end{Bmatrix}$ projectile mass center coordinates (ft)

$\begin{Bmatrix} \tilde{X} \\ \tilde{Y} \\ \tilde{Z} \end{Bmatrix}$ projectile force (lbf)

ε nondimensionalized growth rate per cycle

(ϕ, θ, ψ) projectile body Euler angles

ν kinematic viscosity of liquid (ft^2 s^{-1})

ρ liquid mass density (slug ft^{-3})

$\tilde{\vdots}$ variable in nonrolling system

NO. OF COPIES	ORGANIZATION
1 (PDF only)	DEFENSE TECHNICAL INFORMATION CTR DTIC OCA 8725 JOHN J KINGMAN RD STE 0944 FORT BELVOIR VA 22060-6218
1	DIRECTOR US ARMY RESEARCH LAB IMNE ALC HRR 2800 POWDER MILL RD ADELPHI MD 20783-1197
1	DIRECTOR US ARMY RESEARCH LAB RDRL CIO LL 2800 POWDER MILL RD ADELPHI MD 20783-1197
1	DIRECTOR US ARMY RESEARCH LAB RDRL CIO MT 2800 POWDER MILL RD ADELPHI MD 20783-1197
1	DIRECTOR US ARMY RESEARCH LAB RDRL D 2800 POWDER MILL RD ADELPHI MD 20783-1197

INTENTIONALLY LEFT BLANK.